

# Quantitative Conjunctival Provocation Test for Controlled Clinical Trials

I. Sárándi<sup>1</sup>; D. P. Claßen<sup>2</sup>; A. Astvatsaturov<sup>3</sup>; O. Pfaar<sup>2</sup>; L. Klimek<sup>2</sup>; R. Mösges<sup>4</sup>;

T. M. Deserno<sup>1</sup>

<sup>1</sup>Department of Medical Informatics, Uniklinik RWTH Aachen, Aachen, Germany;

<sup>2</sup>Center of Rhinology and Allergology, Wiesbaden, Germany;

<sup>3</sup>Institute of Medical Statistics, Informatics and Epidemiology, Cologne Ophthalmological Reading and Image Analysis Center, Experimental Ophthalmology, University Hospital Cologne, Cologne, Germany;

<sup>4</sup>Institute of Medical Statistics, Informatics and Epidemiology, University Hospital Cologne, Cologne, Germany

## Keywords

Conjunctival provocation test, allergy, image processing, Hough transform, segmentation, clinical trials

## Summary

**Background:** The conjunctival provocation test (CPT) is a diagnostic procedure for the assessment of allergic diseases. Photographs are taken before and after provocation increasing the redness of the conjunctiva due to hyperemia.

**Objective:** We propose and evaluate an automatic image processing pipeline for objective and quantitative CPT.

**Method:** After scale normalization based on intrinsic image features, the conjunctiva region of interest (ROI) is segmented combining thresholding, edge detection and Hough transform. Redness of the ROI is measured from 0 to 1 by the average pixel

redness, which is defined by truncated projection in HSV space. In total, 92 images from an observational diagnostic study are processed for evaluation. The database contains images from two visits for assessment of the test-retest reliability (46 images per visit).

**Result:** All images were successfully processed by the algorithm. The relative redness increment correlates between the two visits with Pearson's  $r = 0.672$  ( $p < .001$ ). Linear correlation of the automatic measure is larger than the manual measure ( $r = 0.59$ ). This indicates a higher reproducibility and stability of the automatic method.

**Conclusion:** We presented a robust and effective way to objectify CPT. The algorithm operates on low resolution, is fast and requires no manual input. Quantitative CPT measures can now be established as surrogate endpoint in controlled clinical trials.

a predefined threshold value. Each concentration increment is followed by 10 minutes waiting time.

As of today, evaluation of CPT is not standardized by international guidelines. Different scoring systems exist based on subjective criteria, such as itching and visual assessment of the ocular hyperemia. Aiming to objectify CPT, several digital image processing methods have been proposed in the literature [3–8]. Among others, these methods include vessel feature analysis such as density, width, color or branching by means of thresholding, edge detection, fractal analysis or densitometry. Recently, Dogan et al. have provided a more comprehensive review on digital image processing applied to photographic CPT documentation [3].

However, most of these methods either rely on manual input (e.g. marking vessel pixels, selecting the region-of-interest) or assume a standardized image acquisition setup, such as a slit-lamp. Still, the core problem of digital CPT is the design of segmentation and color assessment of the conjunctiva, which must be robust according to imaging resolution, scale, partial occlusions, speckle reflections, and illumination conditions.

In previous work, digital analysis was applied to objectify CPT measurements, and our first work was focused on a four-filter system to enhance color contrast, depict vessel edges and rims, and reduce background noise [3]. This pipeline, however, was error prone due to the manual interaction required in several of the processing steps. In [9], we aimed at further automation of the process but the strictly circular region of interest (ROI) was still determined manually.

## Correspondence to:

Prof. Dr. Thomas M. Deserno  
Dept. of Medical Informatics  
Uniklinik RWTH Aachen  
Pauwelsstr. 30  
52057 Aachen  
Germany  
E-mail: deserno@ieee.org

## Methods Inf Med 2014; 53: 238–244

doi: 10.3414/ME13-12-0142

received: December 12, 2013

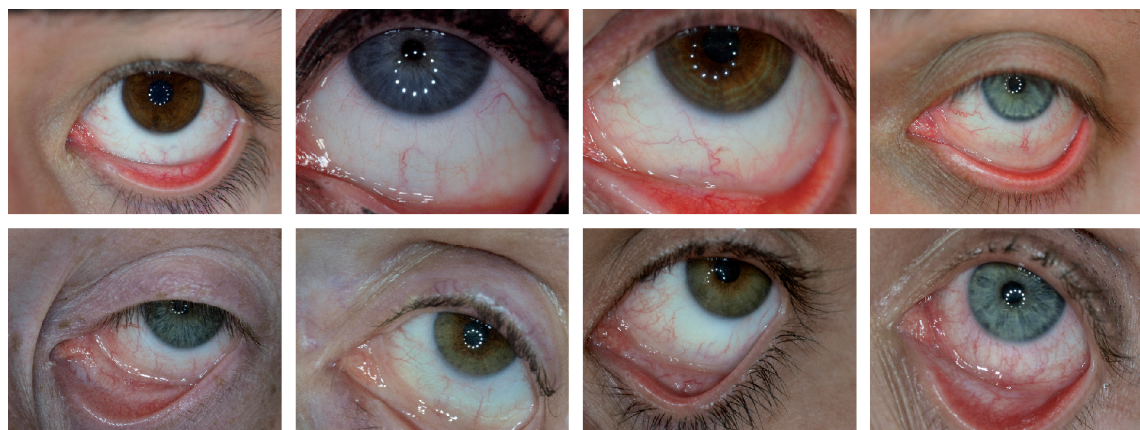
accepted: April 25, 2014

epub ahead of print: June 27, 2014

## 1. Introduction

Allergic rhinoconjunctivitis is a widespread disease of great epidemiologic importance: about 500 million people worldwide are affected by allergic rhinitis, its prevalence is over 20% in most countries, and its associ-

ated health costs are steadily increasing [1]. In general, the conjunctival provocation test (CPT) serves as a model of allergic rhinoconjunctivitis [2]. In CPT, solutions of increasing allergen concentration are administered to the lower conjunctival sac of the eye until the allergic reaction exceeds

**Figure 1**

Digital photography of CPT varies considerably in scale, position, color, contrast, and blur.

In this paper, we propose a self-calibrating fully automatic image processing chain for quantitative CPT. The core concept of this work has been presented at the German Annual Meeting on Medical Informatics and has been published as abstract [10].

## 2. Methods

In this section, we describe the image acquisition, the processing pipeline, the implementation of the algorithm, and the evaluation study performed to prove reliability of our method.

### 2.1 Image Acquisition

During CPT, several images of the patient's eye are acquired with a digital camera. In one eye a control solution, in the other eye an allergen solution is applied. The first image is recorded before administration of any allergen solution and is used as reference in evaluation. After application of the allergen dose, a new image is recorded.

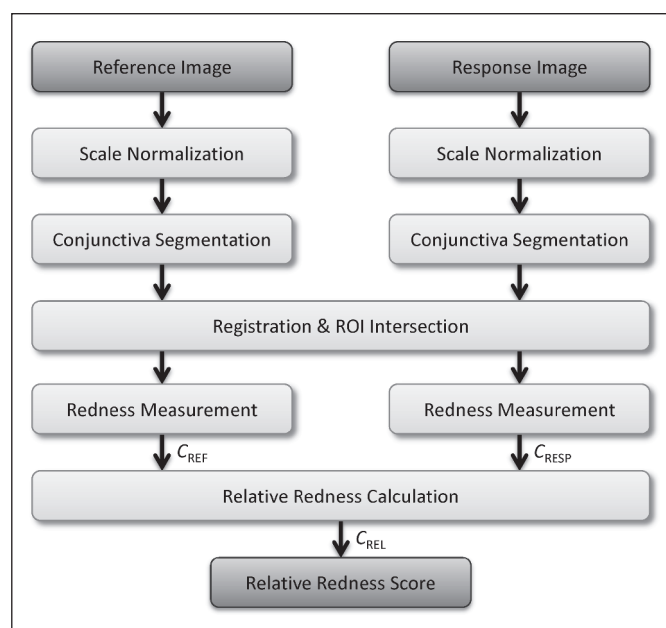
► Figure 1 shows some examples of resulting images, collected from several subjects at different visits. The photographs differ significantly in conjunctiva position and size, color intensity and contrast, focus, noise, and in the direction of view. Hence, automatic image processing must be robustly coping with these variations and effectively self-calibrating for objective and reproducible quantitative measurements.

### 2.2 Image Processing

The input of the processing pipeline is a pair of images of the same eye: one taken before administration of any allergen solution (named henceforth the reference image) and one after application of the dose of allergen, which triggers the allergic reaction (response image). The output of the system is a redness score for both images, from which the quantitative measure for the strength of allergic reaction can be computed by taking their relative difference. The variability in image appearance must be considered when designing a robust algorithm.

The overall procedure we are suggesting is depicted in ►Figure 2: In order to achieve invariance against eye-to-camera distance, scale normalization is applied based on intrinsic image features. Then, the conjunctiva region-of-interest (ROI) is segmented in both images independently, which again relies on robust intrinsic image features. Subsequent registration and intersection of the conjunctiva ROIs ensure that the redness score is calculated over the same subregion of the eye for both the reference and the response image. Finally, redness measurement is performed independently in both registered ROIs. The increase in redness is quantified by the

**Figure 2**  
Overall image processing pipeline



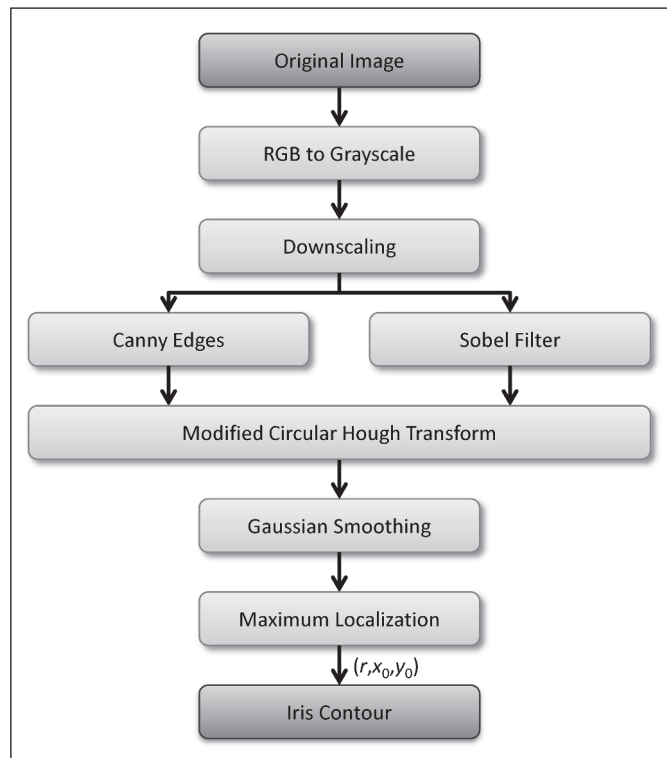


**Figure 3**  
Iris detection

relative difference of the redness values of the reference and response images.

### 2.2.1 Intrinsic Feature Extraction

Due to its circular shape, size, and contrast, the iris is a prominent and robustly detectable intrinsic landmark. Its location is used for the scale normalization and the segmentation step of the pipeline. It is localized using a modified circular Hough transform on the Canny edge map of the image downsampled to 256 px × 192 px resolution (► Figure 3).

Our version of the circular Hough transform uses gradient information obtained by convolution with a Sobel kernel in horizontal and vertical directions. Furthermore, Hough votes are only cast upwards in the image, i.e. only for circle candidates whose center is above the voting pixel [11]. The rationale is that most images do not contain the upper part of the iris circle and voting downwards would lead to spurious votes from the upper eyelid. The Hough space accumulator array is smoothed by an asymmetric sphere Gaussian convolution kernel of  $\sigma_{x,y} = 1.20$  px in  $x_0$  and  $y_0$  direction and  $\sigma_r = 0.75$  px in  $r$  direction to allow robust maximum detection. The circle corresponding to this maximum is regarded as the iris outline (► Figure 5). The Hough transform delivers its radius  $r$  and its center coordinates  $(x_0, y_0)$ .

### 2.2.2 Scale Normalization

Since the photos may be taken at uncontrolled eye-to-camera distance, on different cameras with different lenses and sensors, scale normalization is performed to ensure that the parameterization of later steps of the algorithm will be effective for all cases. Uniform rescaling is applied such that the radius  $r$  of the iris becomes  $r = 170$  px in both of the images. Linear interpolation is used in this step [12].

### 2.2.3 Conjunctiva Segmentation

There are several challenges in designing automatic segmentation of the conjunctiva [5]. First, the border between the conjunctiva formix and tarsi is not always sharp

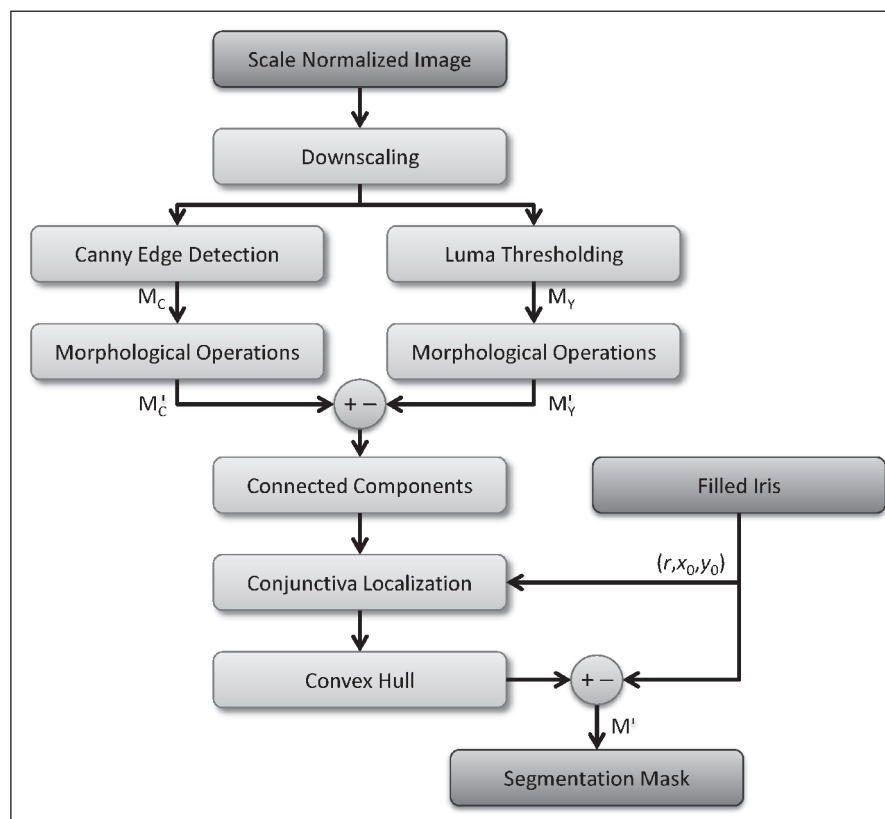


**Figure 4** Conjunctiva segmentation

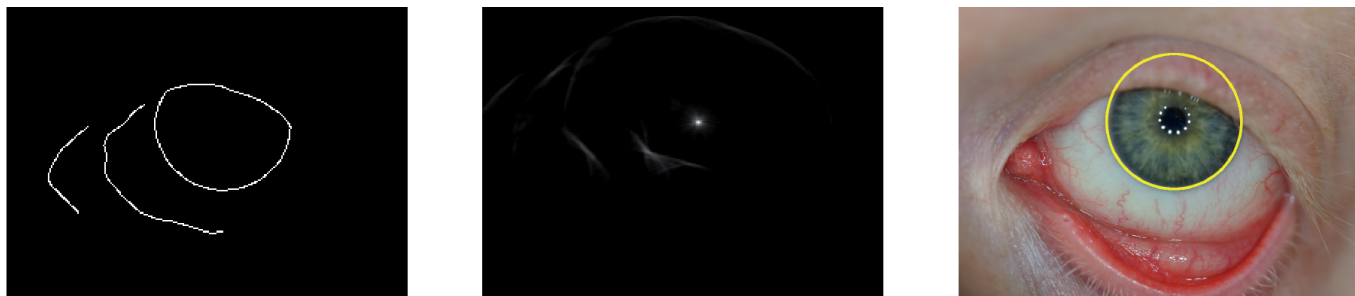


**Figure 5** Example of iris detection. Left: Canny edge map; middle: Hough accumulator array sliced at the radius of the maximum voted bin; right: detected geometry of the iris superimposed to the original image

and sharp edges may also correspond to blood vessels instead of the contour of the conjunctiva. Second, the color and intensity of the conjunctiva varies across individuals and is depending on the allergen dose. Therefore, a threshold-based approach is combined with an edge-based technique (►Figure 4). This also allows to compute the segmentation step on a further downscaled image (iris radius  $r = 50$  px) for efficiency reasons.

For the threshold-based approach, the image is converted from red, green, blue (RGB) color space to YUV color space, where the luminance Y is defined as

$$Y = 0.2126 R + 0.7152 G + 0.0722 B$$

A binary mask  $M_Y$  is acquired by thresholding in the Y channel, which is empirically more distinctive than the grayscale intensity. To determine that threshold, we define a rectangle below and centered to the middle point of the iris. The dimension in width and height are  $3r$  and  $4r$ , respectively, where  $r$  again denotes the iris radius. The threshold is computed as the mean Y value in the cropped rectangle. Noise is re-

moved from the mask by morphological closing and opening with a disk structuring element of radius 1 and 4 respectively, yielding the mask labeled  $M_Y'$ .

Edges are detected by applying the Canny technique (labeled  $M_C$ ). Gaussian blurring is adjusted to  $\sigma = 4$  to avoid the detection of blood vessels. Since edges obtained from the Canny technique are usually disconnected regarding a certain contour such as the conjunctiva, morphological operations are applied to fill gaps between edge pieces: The image is closed with a disk with a radius of 4 px. Next, any remaining isolated edge pieces under the length of 50 px are removed. Then a stronger closing is performed with a disk of radius 8 px. The resulting binary image is labeled  $M_C'$ .

$M_C'$  is then subtracted from  $M_Y'$  to detach false positive areas from the connected component of the conjunctiva. In the resulting binary image

$$M = M_Y' - M_C'$$

the conjunctiva is selected as the adjacent connected component below the iris circle.

The perimeter of the conjunctiva component is subsequently smoothed by a convex hull operation and the iris disk is subtracted again to finally end with the conjunctiva ROI  $M'$ .

►Figure 6 shows some intermediate results of the segmentation step. The top row illustrates a case where the thresholding approach would suffice alone, but the edge-based approach would not (as the contour is discontinuous), while the bottom row shows the opposite case:  $M_C'$  has a continuous contour but the thresholded approach yields false positive areas. The combination of the two approaches ensures correct segmentation in both of these cases.

## 2.2.4 ROI Registration and Intersection

Due to differences in eyelid openness and changes in gaze direction, some parts of the conjunctiva may be exposed in only either of the reference or the response image. In support of a quantitative comparison of the redness in both images, the same part of the eye must be measured. Since the shapes of the ROIs cannot be considered as reliable,



**Figure 6** Example of conjunctiva segmentation. Left to right: original image,  $M_Y$ ,  $M_Y'$ ,  $M_C$ ,  $M_C'$ ,  $M'$

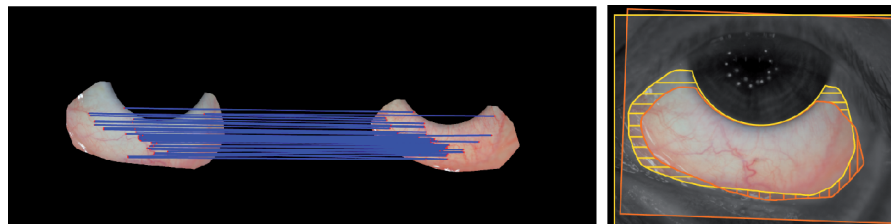


**Figure 7** SIFT based registration. Left: corresponding key points in both images; right: registered masks

the registration should rely on intrinsic features (landmarks). Furthermore, the features must be robust to rotation, translation and scale. Therefore, registration of the reference and response images is performed by the scale invariant feature transform (SIFT) algorithm [13], applied to the RGB images masked with  $M'$ . Key points are localized by the difference-of-Gaussians detector in scale space and the Hessian detector in image space. Random sample consensus (RANSAC) is used for robust estimation of a similarity transformation between the two images [14]. Using this transformation, the reference and the response conjunctiva regions are brought to alignment and their ROIs are intersected such that only common parts remain. This intersection also removes remaining false positive areas, if they had been included in the ROI of only one of the images (►Figure 7), for instance, areas of speckles on the left side of  $M'$  in the reference and the lower side of  $M'$  in the response image.

## 2.2.5 Redness Measurement

Redness is measured independently in the registered and intersected ROIs of the reference and response image as described in our previous work [9]. First the image is transformed from RGB into hue, satu-

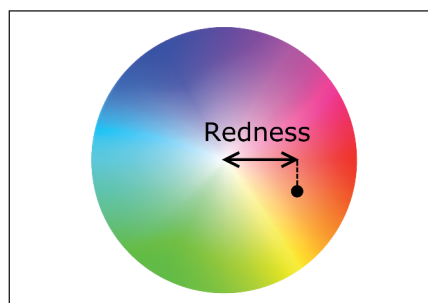


**Figure 8** Definition of color redness illustrated on the hue-saturation polar plane

ration, value (HSV) color space. The redness of any color is defined by its projection onto the red vector in the HSV cylindrical space (►Figure 8).

Negative values are truncated to zero. The redness score  $C$  for the entire ROI is averaged from all pixels in the ROI

$$C = \frac{1}{N} \sum_{i=1}^N \max \{0, S_i \cos(2\pi H_i)\}$$

where  $N$  is the number of pixels in the ROI, while  $H_i$  and  $S_i$  denote the hue and saturation components of the  $i$ -th pixel, respectively. Averaging over the entire ROI yields a measure that is sensitive to both the proportion of vessel pixels in the ROI

and to their color. The range of  $C$  is between 0 and 1. The relative redness score  $C_{\text{REL}}$  is computed as

$$C_{\text{REL}} = \frac{C_{\text{RESP}} - C_{\text{REF}}}{C_{\text{REF}}}$$

where the indices REF and RESP refer to the reference and the response images, respectively.

►Figure 9 illustrates the redness measurement, where each pixel is encoded as gray value in the corresponding ROIs. According to the increased redness, the brightness of the pixels in the response image is increased.

## 2.3 Implementation

The algorithm is developed using the NetBeans IDE (v7.3) in the Java programming language (JDK 7) over the ImageJ public domain image processing platform (v1.46r) [15]. Third party open-source libraries used are ImageScience (v2.4.1) [16], JAMA (v1.0.3) [17], JavaGeom (v0.11.1) [18], customized versions of the FindConnected Regions [19] and JavaSIFT [20] ImageJ plugins and the Google Guava 14.0 general purpose library [21].

## 2.4 Evaluation Study

To evaluate the effectiveness and robustness of our image processing algorithm, images of an explorative pilot study have been used. The database contains 92 images of 23 patients with allergic rhinoconjunctivitis.

The study was aimed at determining the reproducibility level of CPT. The individual test-dose, which evokes the allergic response

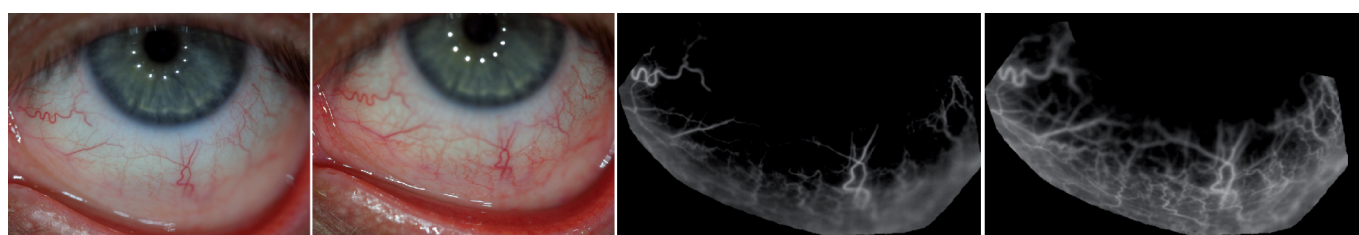


**Figure 9** Redness measurement. Left to right: reference and response images,  $C_{\text{REF}}$  and  $C_{\text{RESP}}$  coded as gray scale

above the predefined threshold, was determined at Visit 1. At Visit 2 and after about four weeks at Visit 3, the individually determined test-dose was applied (the concentration varied across subjects but not across visits). During and between the visits, the subjects got neither any therapy nor any drugs. The database contains four images per subject: one reference and one response image at each of the Visits 2 and 3.

An Olympus PEN E-P1 (Japan) digital camera with an Olympus M. Zuiko Digital ED 60mm f/2.8 macro lens was used. The pixel matrix yields 4032 px  $\times$  3024 px, instantaneously reduced to 1024 px  $\times$  768 px. Controlled illumination was provided by a Hama 12 LED-Macro ring light (Germany) at color temperature of 5,500 K. The subjects placed their heads on a simply constructed chin and forehead rest [3].

We apply the proposed algorithm to determine the redness scores  $C_{\text{REF}}$ ,  $C_{\text{RESP}}$ , and  $C_{\text{REL}}$ . Mean and standard deviation is computed for all  $C$ -scores in both visits separately. Next, the correlation coefficient (Pearson's  $r$ ) is examined between Visit 2 and Visit 3 regarding  $C_{\text{REF}}$ ,  $C_{\text{RESP}}$ , and  $C_{\text{REL}}$ . Repeated measures analysis of variance (ANOVA) is used to test differences in redness measures across  $C_{\text{REF}}$ ,  $C_{\text{RESP}}$ , and Visits 1 and 2.

Furthermore, we compare the relative measures obtained automatically by our algorithm with a relative redness score  $C_{\text{MAN}}$  that has been calculated with MATLAB on manual segmentation.

**Table 1** Statistical evaluation of the test-retest reliability study

	Visit 2		Visit 3		Correlation (Pearson's $r$ )
	Mean	St. dev.	Mean	St. dev.	
Reference redness $C_{\text{REF}}$	0.063	0.043	0.071	0.033	0.535 ( $p < .01$ )
Response redness $C_{\text{RESP}}$	0.174	0.097	0.166	0.086	0.857 ( $p < 10^{-6}$ )
Relative redness $C_{\text{REL}}$	2.430	2.159	1.747	1.536	0.672 ( $p < .001$ )
Manual relative measure $C_{\text{MAN}}$	2.387	1.714	2.339	2.004	0.590 ( $p < .01$ )

### 3. Results

All 92 images were processed successfully with our algorithm. All three scores from both visits correlate statistically significant (►Table 1). The highest correlation is observed for  $C_{\text{RESP}}$  (Pearson's  $r = 0.857$ ,  $p < 10^{-6}$ ). Redness measures showed an overall difference across levels of visits and reference/response scores ( $F(3,66) = 28.41$ ,  $p < 10^{-4}$ ).  $C_{\text{REF}}$  and  $C_{\text{RESP}}$  were significantly different ( $F(1,66) = 84.74$ ,  $p < 10^{-4}$ ), while measures at Visits 2 and 3 were not different ( $F(1,66) = 0.0004$ ,  $p = 0.984$ ).

There was no difference between the automatic relative measures and the manual measures ( $F(3,66) = 1.00$ ,  $p = 0.398$ ). Linear correlation (Pearson's  $r$ , ►Table 1) of the automatic measure ( $r = 0.67$ ) is larger than the manual measure ( $r = 0.59$ ), which indicates a higher reproducibility and stability of the automatic method.

►Figure 10 illustrates automatic vs. manual measures in the test-retest evaluation experiment. The box plots (►Figure 10, left) indicate a slightly larger standard deviation of the automatic method

(►Table 1), while the scatter plots (►Figure 10, right) depict the improved linear correlation of the automatic method.

### 4. Discussion

A simple and robust, fully automated image processing chain has been proposed for objective evaluation of the CPT. The effectiveness of our approach is confirmed by evaluation on the database of a test-retest reliability study. With our approach, quantitative CPT measures can be established as surrogate endpoints in controlled clinical trials, where robustness and reproducibility of automatic computations will reduce the number of subjects to be included and hence, the costs of such trials.

Basically, our algorithm consists of three steps: i) ROI extraction, (ii) ROI alignment, and ii) relative redness determination. Previous approaches to automated measurement of bulbar redness mainly rely on rectangular boxes that are extracted manually as ROI. For instance, rectangles such as 500  $\times$  400 and 400  $\times$  300 pixels [8] and

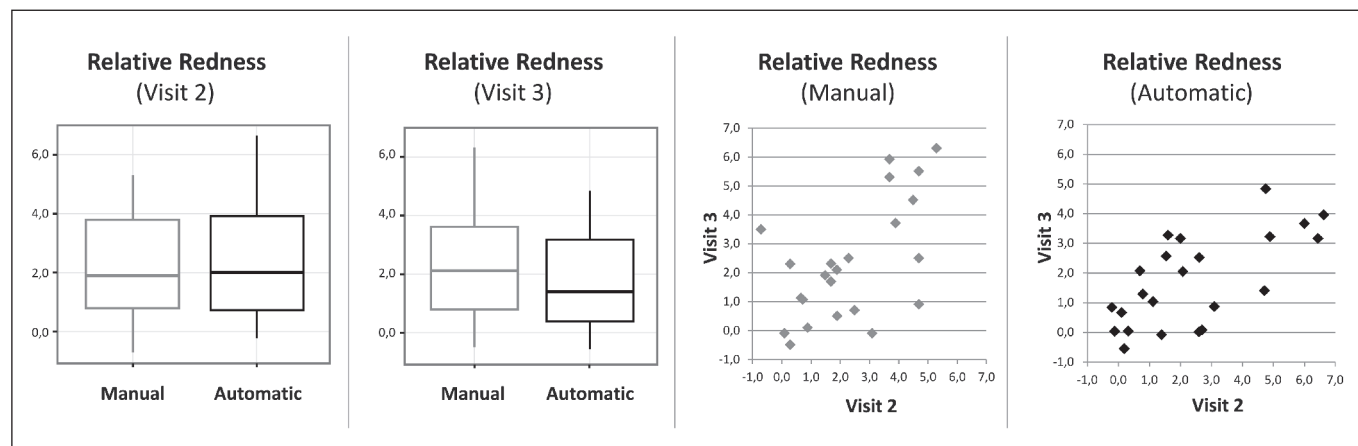


**Figure 10** Graphical visualization of the test-retest reliability study

3.2 mm × 2.5 mm [6] or squares of 300 × 300 pixels [7] and 230 × 230 pixels [6]. Our previous work is based on circular arc-shaped ROIs [9]. Here, in contrast, the entire conjunctiva is extracted following its morphologic boundary, which is detected automatically combining Hough transform, Canny edge detection, and morphological operations on thresholded images.

To the best of our knowledge, fully automatic ROI extraction and alignment has not yet been performed. Contrarily in previous works, the images presented for instance by Fukushima and Tomita [7] clearly depict a ROI displacement over the measurements taken consecutively within eight minutes from a guinea pig model. Such misalignments, naturally occurring also with manual ROI extraction, increase the variance in quantitative measures and reduce the reliability of the image analysis chain.

In the majority of previous work, redness was determined based on the vessels, which are observed to widen on provocation and hence, increase redness. Initially, Fieguth and Simpson used the length measured by a relative count of Canny edge pixels. Then, Owen, Ellis and Woodward suggested the width of vessels being more robust [6], while Yoneda et al. [8] and Fukushima and Tomita [7] have attempted to assess both, width and length simultaneously by simply integrating over thresholded vessel pixels and applying a more sophisticated fractal analysis, respectively. However, Fieguth & Simpson already stated that small arteries are resolvable neither by the pixels in a charge-coupled device (CCD) camera, nor by the human eye, and a mild onset of hyperemia therefore begins as a diffuse reddening with no discernible edges [5]. In such cases, they have proposed an integrated measure of redness, as it is used in our approach, too. Disregarding the edges of the vessels is furthermore advantageous for analyzing defocused images, which may result from consumer and smartphone cameras. Note that due to the limited focus depth in optical macro imaging, vessels near the surface of the sphere-shaped conjunctiva will always be defocussed at either their ends. Integrated measures will also support non-standardized eye-to-camera distance and varying pupil positioning.

The algorithm proposed in this paper predominantly consists of simple operations such as thresholding, edge detection and morphological operations. The computationally more expensive processing steps such as the circular Hough transform are performed in lower resolution yielding an efficient and fast algorithm. In line with Fukushima and Tomita [7], our implementation is based on ImageJ (available at: <http://rsb.info.nih.gov/ij/>), distributed by the National Institutes of Health, and other Java libraries. On average, a pair of 1 M px images is processed with all steps of the proposed pipeline in 3.44 s ± 0.58 s (measured on an Dell inspiron 7720 computer equipped with Intel® core™ i7-3630QM CPU @ 2.40 GHz). This enables the integration of the entire image capturing and analysis process into a smart device such as a smart phone. Furthermore, images and/or measurements can be transferred directly into an electronic case report form using web services [23]. Although a generalized usability of the proposed method still needs critical examination, our future aim is constructing an integrated mobile Health application [24], by which a smartphone is converted into a medical diagnostic device if simply an app is installed [25, 26].

mine-induced conjunctivitis in guinea pigs. Cornea 2009; 28: 694–698.

8. Yoneda T, Sumi T, Takahashi A, Hoshikawa Y, Kobayashi M, Fukushima A. Automated hyperemia analysis software: reliability and reproducibility in healthy subjects. Jpn J Ophthalmol 2012; 56: 1–7.
9. Bista SR, Sárándi I, Dogan S, Astvatsaturov A, Mösges R, Deserno TM. Automatic conjunctival provocation test combining Hough circle transform and self-calibrated color measurements. Proc SPIE 2013; 8670: 2J1–0.
10. Sárándi I, Deserno T, Classen D, Pfarr O, Astvatsaturov A, Mösges R. Quantitative conjunctival provocation test. In: Proceedings GMDS 2013, German Medical Sciences. <http://www.egms.de/static/en/meetings/gmds2013/13gmds074.shtml>
11. Lehmann TM, Kaupp A, Effert R, Meyer-Ebrecht D. Automatic strabometry by Hough-transformation and covariance-filtering. In: Proceedings ICIP-94. IEEE Computer Society Press, Los Alamitos, CA, 1994; 1: 421–425.
12. Lehmann TM, Gönner C, Spitzer K. Survey: Interpolation methods in medical image processing. IEEE Trans Med Imaging 1999; 18 (11): 1049–1075.
13. Lowe DG. Distinctive image features from scale-invariant keypoints. Int J Comput Vis 2004; 60 (1): 91–110.
14. Fischler MA, Bolles RC. Random sample consensus: a paradigm for model fitting with applications to image analysis and automated cartography. Comm ACM 1981; 24 (6): 381–395.
15. Abramoff MD, Magalhaes PJ, Ram SJ. Image processing with ImageJ. Biophoton Int 2004; 11 (7): 36–42.
16. Meijering E. Imagescience.org. [Online]. Cited 2013 11 26. Available from: <http://www.imagescience.org/meijering/software/featurej/releases/>.
17. Hicklin J. JAMA website. [Online]. Cited 2013 11 26. Available from: <http://math.nist.gov/javanumerics/jama/>.
18. JavaGeom. [Online]. Cited 2013 11 26. Available from: <http://geom-java.sourceforge.net/>.
19. Longair M. Find Connected Regions Plugin. [Online]. Cited 2013 11 26. Available from: <http://www.longair.net/edinburgh/imagej/find-connected-regions/>.
20. Saalfeld S. JavaSIFT. [Online]. Cited 2013 11 26. Available from: <http://fly.mpi-cbg.de/~saalfeld/Projects/javasift.html>.
21. Bourrillion K. Guava: Google Core Libraries for Java 1.5+. 2010.
22. Haak D, Jonas S, Gehlen J, Deserno TM. OC To-go: on patient's site integration of images into OpenClinica in clinical trials by mobile devices. Proc SPIE 2014; 9039: in press.
23. Laakkonen T, Leppänen J, Lähteenmäki J, Nummiahko A. Mobile health and wellness application framework. Methods Inf Med 2008; 47 (3): 217–222.
24. Labrique A, Vasudevan L, Chang LW, Mehl G. H\_ope for mHealth: more “y” or “o” on the horizon? Int J Med Inform 2013; 82 (5): 467–469.
25. Struzik ZR, Yoshiuchi K, Sone M, Ishikawa T, Kikuchi H, Kumano H, Watsuji T, Natelson BH, Yamamoto Y. “Mobile Nurse” platform for ubiquitous medicine. Methods Inf Med 2007; 46 (2): 130–134.

## References

1. Pawankar R, Canonica GW, Holgate ST, Lockey RF (eds). WAO White Book on Allergy. Milwaukee, WI, USA: World Allergy Organization (WAO); 2011. ISBN 978-0-615-46182-3.
2. Riechelmann H, Epple B, Gropper G. Comparison of conjunctival and nasal provocation test in allergic rhinitis to house dust mite. Int Arc Allergy Immunol 2003; 130 (1): 51–59.
3. Dogan S, Astvatsaturov A, Deserno T, Bock F, Shah-Hosseini K, Michels A, et al. Objectifying the Conjunctival Provocation Test: Photography-Based Rating and Digital Analysis. Int Arch Allergy Immunol 2013; 163 (1): 59–68.
4. Horak F, Berger U, Menapace R, Schuster N. Quantification of conjunctival vascular reaction by digital imaging. J Allergy Clin Immunol 1996; 98: 495–500.
5. Fieguth P, Simpson T. Automated measurement of bulbar redness. Invest Ophthalmol Vis Sci 2002; 43: 340–347.
6. Owen CG, Ellis TJ, Woodward EG. A comparison of manual and automated methods of measuring conjunctival vessel widths from photographic and digital images. Ophthalmic Physiol Opt 2004; 24: 74–81.
7. Fukushima A, Tomita T. Image analyses of the kinetic changes of conjunctival hyperemia in hista-